



BACHELOR PROJECT: THE DA VINCI-INSPIRED DESIGN CHALLENGE

ME-314

Leonardo da Vinci's gearbox



MEYER Quentin 315970

CANOEN Louis 312526

GRIFFON Pierre 316216

LAVINE Salomé 311643

October 30, 2025

Table of contents

1 Abstract	2
2 Introduction	2
2.1 Contributions to the project	2
3 Methods of building and experiments	4
3.1 Design plan	4
3.2 Building of the gearbox	5
3.2.1 Comment on the material	5
3.2.2 Gears, axles and washers	5
3.2.3 Walls and keys	7
3.3 Experiments	7
3.3.1 Thermal camera	7
3.3.2 Friction experiment	8
3.4 Difficulties	9
4 Results and discussion	10
4.1 Theory	10
4.1.1 Rotational speed modeling	10
4.1.2 Thermal analysis	15
4.1.3 Finite element analysis	22
4.2 Results	26
5 Conclusion	28
6 Acknowledgement	28
7 Bibliography	29
8 Appendix	30

1 Abstract

"The sun, which heats the whole world, will seem cold and motionless compared to this instrument" - Leonardo da Vinci

Leonardo da Vinci's gearbox thought experiment was to generate high temperatures through friction with a rotating gear. This study will investigate its feasibility as well as his hypothesis on its ability to generate high temperatures. Through experimental analysis and modeling, we assessed the torques, angular velocities and heat generation of his idea. Our findings indicate how inefficient his design was. Moreover we found how important more advanced friction and heat generation models are. This results highlight the need for more advanced analysis when it comes to friction forces in complex and extreme systems. Future research should focus on the impact of different materials used in the device in order to extract models more in line with the industry.

2 Introduction

Leonardo da Vinci had many ideas for devices that ended up being perfected after his time, but some of them were more thought experiments rather than real physical inventions. This study will aim to address the feasibility of one of his unknown gearbox from his codex *Atlanticus* designed as a velocity multiplicator to generate high temperatures by friction with the last gear surface. Few studies exist when it comes to computing heat generation, and friction modeling in high velocity gear assemble.

Between our mechanical engineering background acquired throughout our Bachelor at EPFL and the lack of public knowledge on this invention, this project was a perfect fit for us.

We had three main objectives for this project. Firstly, to model and analyze the contact temperature between the teeth of two successive gears for different speeds and applied forces. Secondly, to model the contact temperature between the surface of our fastest gear and a wooden dowel. Finally, to determine the force required to rotate our gearbox with as many gears as possible.

2.1 Contributions to the project

- MEYER Quentin: Modeling and analysis of torques and angular velocities.
- CANOEN Louis: Designing of the gear box and finite element modeling.

- LAVINE Salomé: Thermal modeling and analysis.
- GRIFFON Pierre: Construction of the box and project video.
- Collective: Redaction of the study and experiments.

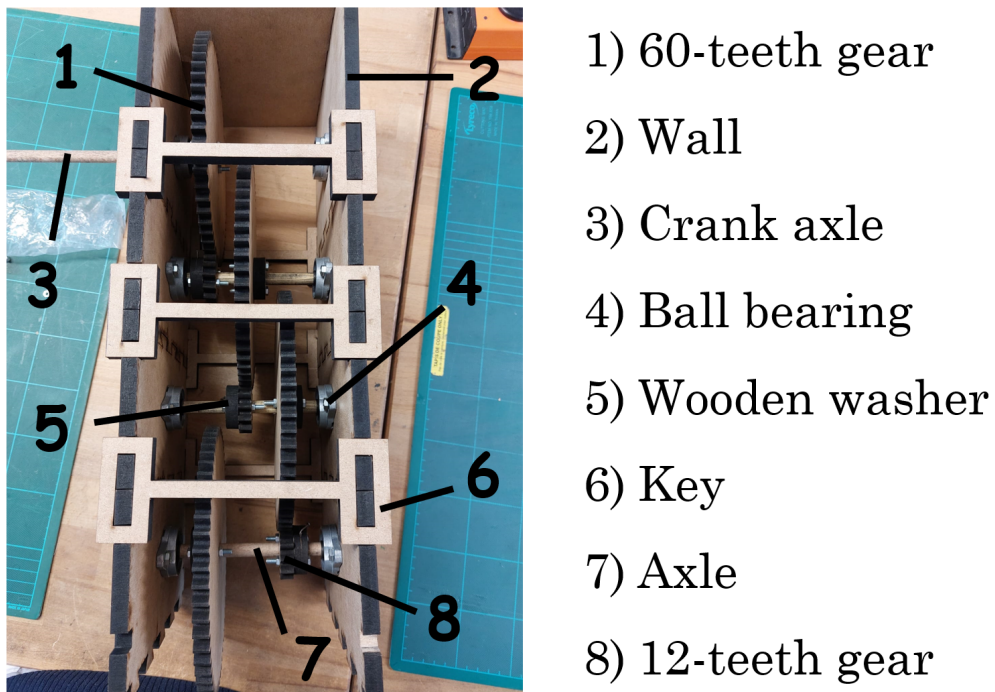
3 Methods of building and experiments

3.1 Design plan

The goal of the experiment is to translate da Vinci's sketch into a real life machine. Firstly, the handling (portability, assembly and disassembly, etc.) of this new contraption should be simple. Secondly, it needs to be tailored to take reproducible measurements with different total gear ratios. The machine is structured with a first crank-module and easily removable sub-modules in order to change the total gear ratio. Each module multiplies the gear ratio by 5. They are composed of two parallel walls which support a single axle on which one 60-teeth gear and one 12-teeth gear are mounted. The edges of the walls are shaped like trapezoids to nest the modules together like a puzzle one after the other. The gears and axles rotate around a horizontal axis.

The gears and axle spin in synchronisation as a solid piece, which is fitted through two ball bearings on the inner sides of the walls. The loss of power due to unwanted friction on the walls will reduce the angular velocities of the gears.

Figure 1: Diagram and legend of the gearbox (top view).

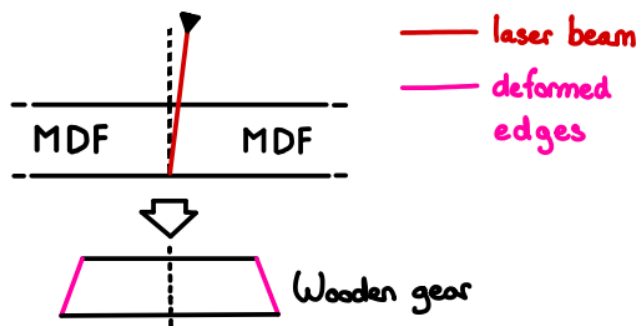


3.2 Building of the gearbox

3.2.1 Comment on the material

Medium Density Fibreboard wood (MDF) is an abundant material at EPFL prototyping facilities and is easily worked on. Laser cutting machines can cut wooden parts such as gears with great precision. Despite their good (x,y) accuracy, the precision along the z-axis decreases as the thickness of the wood increases. The laser beam is not perfectly vertical and is slightly crooked (see figure 2) which is all the more visible as the thickness increases. Due to the nature of the laser cutting technology, the speed of the nozzle decreases with thickness since the laser needs more time to fully go through the wood. Different thicknesses ranging from 5 mm to 10 mm were available. The final decision was to take 10 mm as our general thickness for every part. The contact surface between the teeth of the gears needed to be as large as possible in order for the teeth to withstand high contact pressures. Secondly, thicker parts means that the gearbox will be sturdier.

Figure 2: Deformed edges induced by the angle of the laser beam.



The deformation of the gear is greatly exaggerated for illustration purposes.

3.2.2 Gears, axles and washers

Attempting to build a mechanism as close as the original idea was not an easy task. Da Vinci mentions that he wishes a gear ratio of 1:20 which means that the output spins 20 times faster than the input speed which is unfeasible. The second gear would measure 800 mm diameter, if the first gear measures 40 mm.

When designing the gears, the shape and number of teeth is a crucial step. The teeth could start interfering with each other if the pressure angle (see figure 3) is too aggressive. There exists a formula¹ which links the maximum number of teeth of the pinion is able to drive without causing interference prematurely, which causes damage:

¹Systèmes mécaniques, Pr. S. Soubielle, 2021-2022

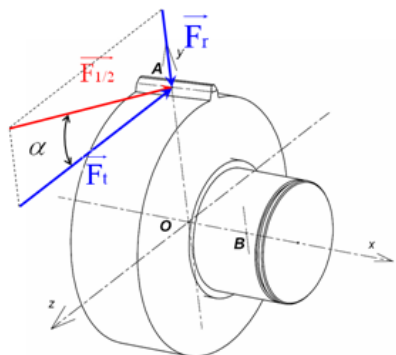
$$Z_{max} = \sqrt{Z_1^2 + 4 \frac{Z_1 + 1}{\sin^2(\alpha)}} - Z_1$$

Where α is the pressure angle of two teeth, Z_1 the number of teeth of the first gear and Z_{2min} the minimum possible number of teeth of the driven gear.

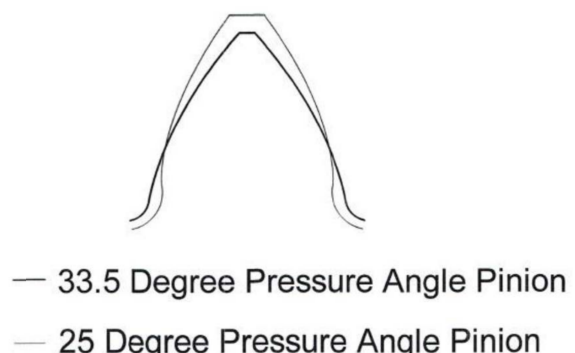
Table 1: Minimum number of teeth for the driven gear according to α ($Z_1 = 60$)

α [deg]	20	21	22	23	24	25
Z_{2min}	16	15	14	13	12	11

Figure 3: Illustrations of the pressure angle α .



(a) Source: Pierre Provot,
Wordpress.



(b) Source: www.geartechology.com.

A pressure angle of 25° would be needed enough to fit a 12-teeth to ensure a 1:5 gear ratio. As the 1:20 was not practical, we took the liberty to decrease it to 1:5. Two gear assemblies would give a ratio of 25 (1:5 times 1:5 is 1:25) comparable to 20. Consequently the diameter of the second gear changes from 80 cm to 20 cm which is much more reasonable for manufacturing and experimenting.

In our initial testing, the gears did not have enough grip around the axles and spun independently. Tightening the gears around the axles was not enough as MDF is too soft and the connection would break. For this reason a wooden washer was fitted alongside every gear. The gear and its washer would attach with nuts and bolts and a thin nail would be driven through the washer and the axle, motion induced by contact being more reliable in the long term.

The diameter of the axles, also made out of MDF, measure 10 mm, the widest dowels that would fit in the ball bearings. Their length is 130 mm which is the distance between one wall to another, long enough to fit two gears and two wooden washers with safety distances between each.

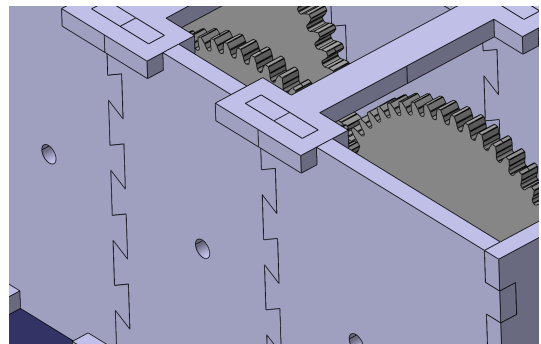
3.2.3 Walls and keys

Two options were available for the walls to be easily assembled and disassembled together. The walls could be fastened together thanks to nuts and bolts or with traditionally Japanese inspired wood joinery(see figure 4). The second option seemed optimal since it would save time during assembly as sliding the wooden pieces together requires less time than tightening nuts and bolts.

Figure 4: Source of inspiration for our design.



(a) Source: Spoon & Tamago.



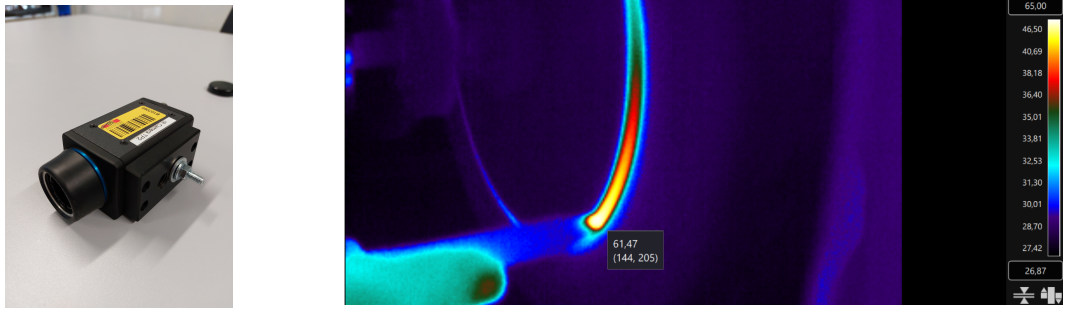
(b) Side view of our gearbox.

3.3 Experiments

3.3.1 Thermal camera

A thermal camera (or IR camera to be exact) is used in order to monitor the temperatures of the contact point between two gears wheels and the contact point between the wooden dowel and the sides of the gears.

Figure 5: Instrumentation used for the experiment.



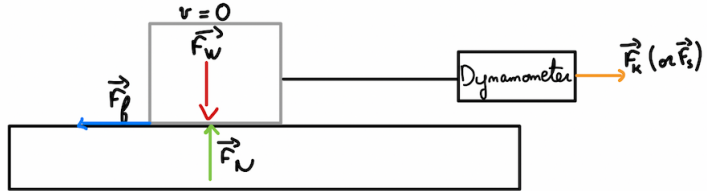
(a) Thermal camera.

(b) Possible result with the thermal camera.

3.3.2 Friction experiment

To model our system as accurately as possible, we decided to carry out an experiment to determine the static and kinetic friction coefficients of the wood used to build the gear box.

Figure 6: Experiment to determine our friction coefficients.



Using a dynamo-meter, we assessed the minimum static force F_s (and kinetic force F_k) required to set (and to respectively keep) the MDF wood block in motion on a board of the same material. We repeated this experiment to increase its precision.

Table 2: Recorded static friction and kinetic forces.

F_s	5.5	5.034	6.1	4	3	3.5	5.622	3.4	5.7
F_k	2.6	2.6	2.7	3	2.7	3	2.7	2.7	2.6

Therefore the mean force is $F_s = 4.61 \text{ N}$ and $F_k = 2.7 \text{ N}$, F_n being equal to the weight of our block is expressed as $F_n = m \cdot g = 9.81 \text{ N}$. Using the following formulas: $\mu_s = \frac{F_n}{F_s}$

and $\mu_k = \frac{F_n}{F_k}$ we obtain a coefficient of static friction $\mu_s = 0.47$ and of kinetic friction $\mu_d = 0.28$, close to the theoretical coefficients between two blocks of wood, 0.5 and 0.3 respectively.

3.4 Difficulties

More experiments such as a flexion test on the teeth of the gears and a torsion experiment for the axles would be useful but were scraped due to the lack of correct equipment and time. MDF also proved to be fragile for this experiment and greatly limited the range of torques we could exert: a crank was originally present on the gear box but its axle split under the high load (see figure 7).

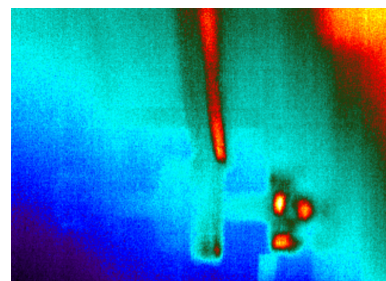
Figure 7: Damage caused by the fragility of MDF.



(a) Split in the crank axle. (b) Broken teeth on one gear.

We also encountered difficulties with the outer surfaces of the gears (see §3.2.1) such as uneven temperature gradients on the teeth (see figure 8) as well as premature wear on the teeth(see figure 8).

Figure 8: Uneven temperature due to surface geometry.



4 Results and discussion

4.1 Theory

Table 3: MDF properties.

Density ρ [kg/m^3]	750
Young's modulus E [MPa]	2'500
Poisson coefficient ν [-]	0.24
Ultimate tensile strength [MPa]	31
Specific heat capacity c_p [$J/(kg \cdot K)$]	1700
Thermal conductivity k [$W/(m \cdot K)$]	0.3

4.1.1 Rotational speed modeling

In this section, we will explain the gear box model with the forces exerted and the speeds generated by the gearbox. To compute the resistance generated by the rotation of the gears, the different forces were separated : fluid resistance generated by the rotation of the gear and the contact friction between the teeth of the gears. The friction generated by the ball bearing will be considered negligible in this analysis.

Moment of Inertia

To calculate the total moment of inertia of one module, we add together the moment of inertia of each rotating part which are the 60-teeth gear, the 12-teeth gear and the axle. These values were obtained from *Catia V5*. In order to add more modules to the system, we multiply the moment of inertia of each successive module by 5^{n-1} with n corresponding to the module.

Contact friction

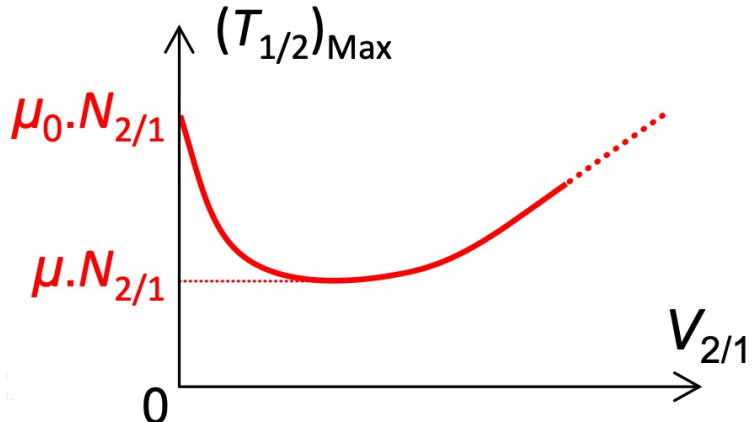
Throughout our research, we found many models for contact friction with varying complexity, We had to find a realistic friction model that underlines heat dissipation.

Discussion with Pr.Molinari

This brought us to discuss with Pr. Molinari, specialized in the numerical modeling of the mechanics of materials and structures. He explained how the friction coefficient

behaves with high velocity. The friction coefficient (static and dynamic) aren't intrinsic properties of a material, but depends on the geometry, surface roughness, velocity, gear meshing characteristics and deformation of the objects in contact.

Figure 9: Friction coefficient depending on velocity.



Graph from the course, Système Mécanique given by Pr. S. Soubielle at EPFL.

To conclude, we decided to analyze the friction of our gear box with the Coulomb friction law ($F_f = \mu \cdot N$), and to use a constant dynamic friction coefficient in order to simplify calculations.

$$M_c = \frac{M \cdot \mu_d}{\cos(\alpha)}$$

With α , the pressure angle and M , the moment exerted.

Fluid resistance

The friction torque of a rotating cylinder against air can be derived by considering the shear stress of it with the air. We found it would lead to a friction torque which was too low because gears are not smooth. Surprisingly, we found that taking the drag equation for a cylinder with linear motion led to the sum of friction forces more comparable to a rotating gear as it compensated for other factors. It is expressed as:

$$M_f = 0.5 \cdot \rho \cdot A \cdot C_d \cdot \omega^2 \cdot r^3$$

Where, ω is the angular velocity, r is the radius of the gear, A is the projected area taken as $A = \pi r^2$, ρ is the density of the air and C_d , the drag coefficient. Computing the true value of C_d for a gear would have been over complicated for this study. We will choose a value of 0.2 (comparable to a smooth sphere moving through a fluid). This approximation might lead to important errors when computing for extreme speeds.

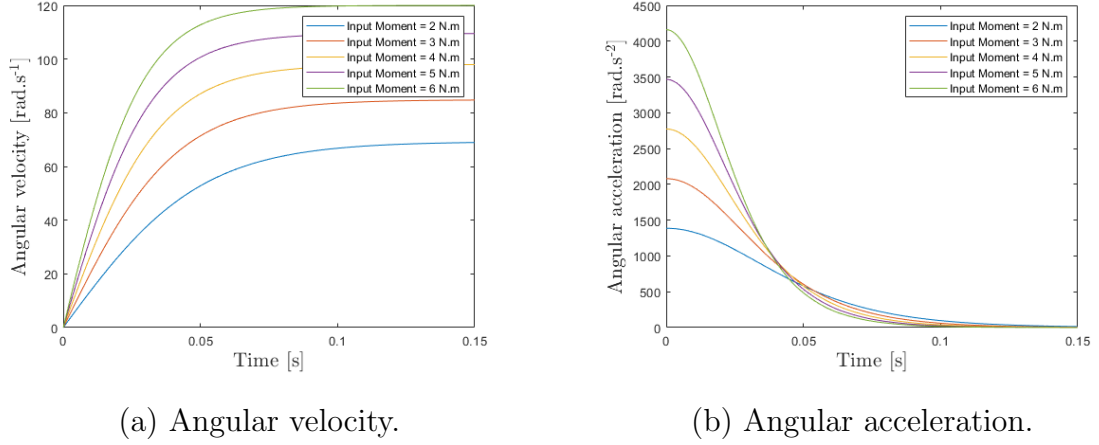
Simulation

The angular acceleration and angular velocity of the first gear are calculated by solving a differential equation taking into account the torque M exerted at the first gear:

$$\dot{\omega}_1 = \frac{M - M_f - M_c}{I}$$

ω the angular speed for this gear. We can then plot the acceleration and angular velocities of the final gear for different numbers of modules and values of M .

Figure 10: Angular velocity and acceleration of the final gear for $n = 4$ modules.



The angular velocities computed with the conditions used during the physical experiments are comparable to what was obtained empirically (see table 4): our model is relatively accurate for small torques and few modules.

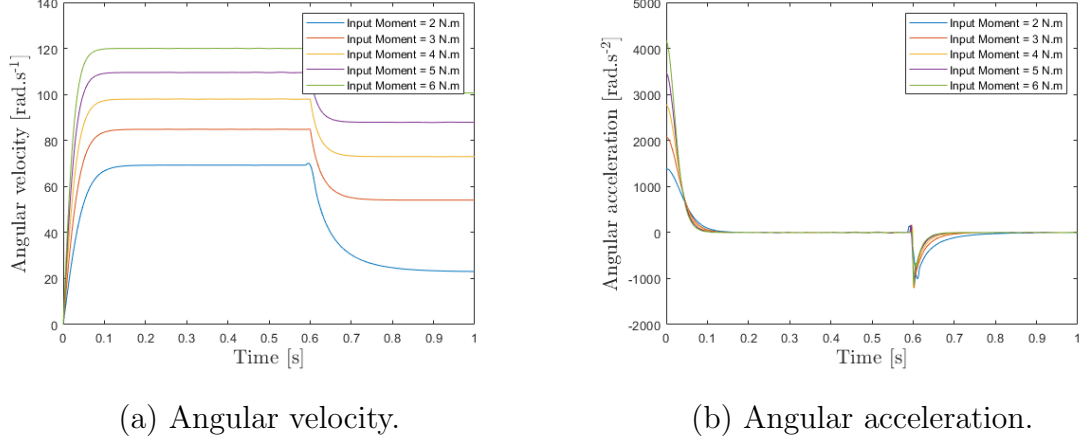
Table 4: Angular velocities for $M \approx 5$ [$N \cdot m$] and $n = 4$.

Gear position	Theoretical angular velocity [$rad \cdot s^{-1}$]	Experimental angular velocity [$rad \cdot s^{-1}$]
1	0.8762	~1
2	4.3812	~5
3	21.9060	~25
4	109.5298	~125

We can then add the friction moment generated by the wooden dowel in contact with the final gear, comparable to the setup used in the experiments. We will assume that

a new normal force of 1 N is applied onto the gear's surface after three fourth of the simulation time span.

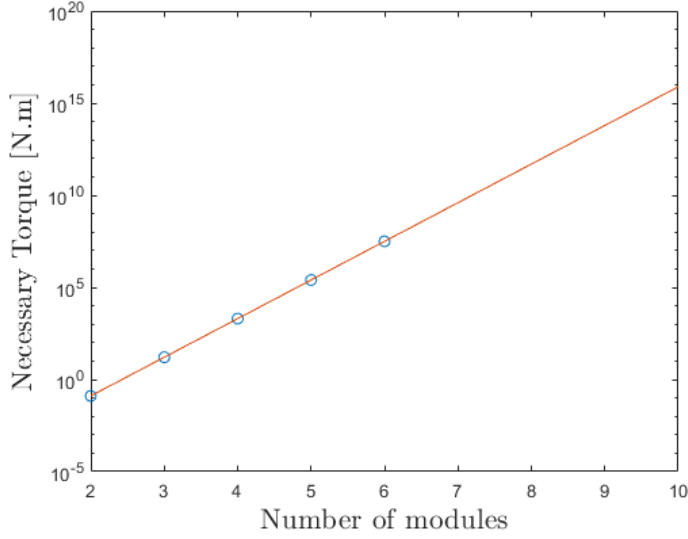
Figure 11: Angular velocity and acceleration for $n = 4$ modules and contact after three fourth of the time span.



We find an upward spike of velocity after the contact but we can assume it to be errors due to how the program calculates the angular velocities.

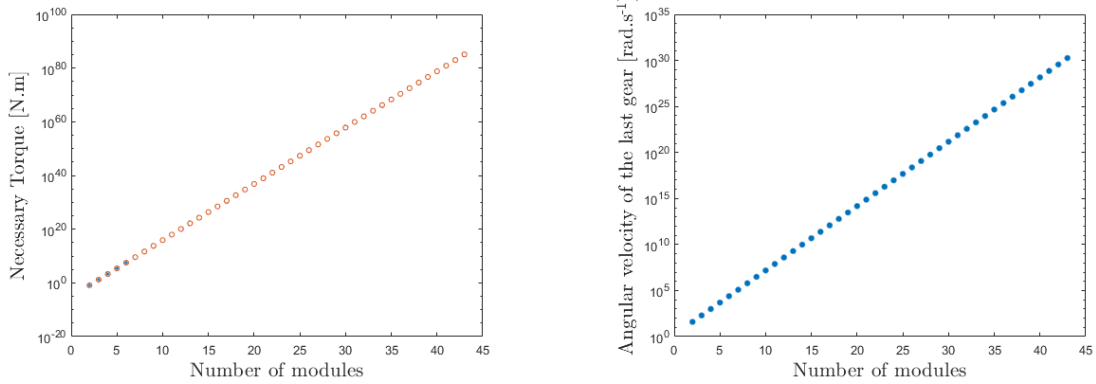
We would like to know the force required to put in motion da Vinci's initial idea, but the model is not viable for values of this magnitude. Inputting the minimal torque required to run the gearbox would not be very interesting since it would just lead to an angular velocity close to zero. We will therefore calculate the moment required to turn the first gear of the device with an angular velocity $\frac{\pi}{2}\text{ rad} \cdot \text{s}^{-1}$ for a varying number of modules. The function which approximate the relationship between the required torque and the number of modules is $f(n) = 10^{2.097n-6.085}$.

Figure 12: Approximation of the necessary torque as a function of n.



Da Vinci had a gear ratio of 1:20 and 23 gears, which is comparable to 43 gears of ratio 1:5 in terms of total gear ratio. This would require a torque of $1.2 \cdot 10^{85} N \cdot m$ and it would reach an angular velocity for the last gear of $1.8 \cdot 10^{30} rad \cdot s^{-1}$.

Figure 13: Required torque and angular velocity generated.



(a) Torque required to rotate the first gear at a speed of $\frac{\pi}{2} rad \cdot s^{-1}$.

(b) Angular velocity of the last gear with $\frac{\pi}{2} rad \cdot s^{-1}$ for the first gear.

The power that would be required by the gear box, $M_{lastgear} \cdot w_{lastgear} = 1.9 \cdot 10^{85} W$ would be more powerful than $1.9 \cdot 10^{40}$ gamma-ray bursts (GRB). These are brief and intense bursts of gamma-ray radiation that occur in distant galaxies. They are associated with the most energetic explosions in the universe ($10^{44} W$). One GRB every second since the Big Bang is still less powerful than what we require. This would probably lead to the creation of a black hole, it is completely unfeasible to attain with human technology.

4.1.2 Thermal analysis

In this section, a change of referential coordinate system (Figure 14) is needed to do a one-dimension thermal analysis. The observer is attached to the gear wheel does not rotate but the surrounding air becomes an air flow with a velocity of the rotation speed times the radius of the gear wheel. All the theory of heat and masses transfer is based on the course of Pr G. Tagliabue. All the rotation velocities, in this section, refer to the theoretical angular velocities of table 4.

Figure 14: Schematic of the referential change.

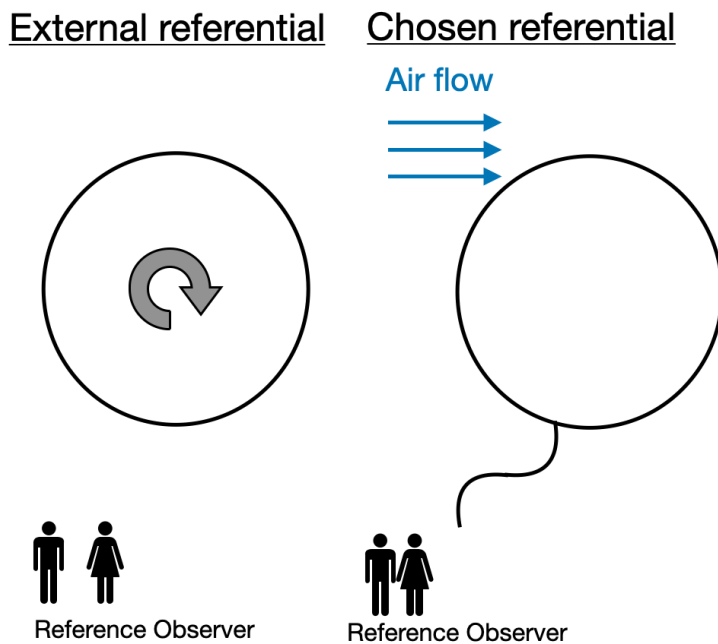


Table 5: Thermal properties of air at environmental temperature, pressure during the experiments.

Thermal properties	T [K]	$k \cdot 10^3$ [W/m · K]	$\alpha \cdot 10^6$ [m ² /s]	Pr [-]	$\nu \cdot 10^6$ [m ² /s]
air	295.65	25.952	21.9	0.708	15.50

interpolation of figure 30 (§8).

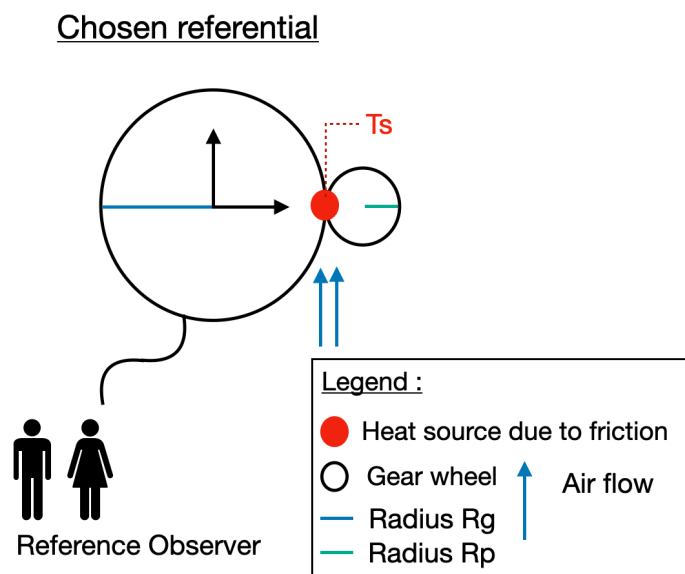
Conduction

First, a list of assumptions to focus on the conduction threw a gear wheel:

- The system is in steady state
- The conduction is in one dimension and only radial
- The contact resistance between the teeth are negligible
- The contact resistance between the teeth are negligible
- The properties of the wood are constant
- A gear wheel are simplified as cylinder
- Radiation is neglected (due to the small diffusivity)

In this section, the focus is to determine the radial temperature profile in a gear wheel due to conduction, by using the chosen referential.

Figure 15: Schematic explain the referential chosen for the conduction analysis.



The heat source due to the friction between two teeth of a gear is modeled by the friction Coulomb's law (see §4.1.1) $F_f = \mu_d \cdot N$, μ_d calculated experimentally (see §3.3.2), N the normal force between two teeth. The heat transfer \dot{Q} (a power) is only due to the friction power: $\dot{Q} = F_f \cdot v = \mu_d \cdot \omega \cdot R$, R gear wheel's radius, ω the rotation speed of the gear.

The thermal radial profile of a one-dimension conduction system in steady state, with a heat source and in radial coordinates,(by using the heat transport law) is :

$$T(r) = -\frac{\dot{q}}{4k} \cdot r^2 + C_1 \cdot \ln(r) + C_2$$

The heat flux \dot{q} is transmitted by the friction force between the teeth: $\dot{q} = \frac{\dot{Q}}{A_t}$, where A_t is the surface of one tooth. First, with the Robin boundary condition, (convection boundary condition, §8 figure 28), we can compute C_1 :

$$-k \left(\frac{\partial T}{\partial r} \right) = h(T_s - T_{inf})$$

With, h , the convection coefficient, T_s the temperature surface at the point of contact. The temperatures surfaces are given by the experiments with the thermal camera (see §4.2).

$$C_1 = R_{max} \frac{h(T_s - T_{inf})}{-k} + 2\dot{q} \frac{R_{max}}{4k}$$

To determine h , the convection coefficient, we have to focus on the air flow, and use the correlation with an external forced convection (control by the input moment). We assume a constant external flow rate and that a gear wheel is a simple thin cylinder. The environmental temperature is $T_a = 22.5^\circ C = 295.65 K$.

$$\bar{Nu}_d = 0.3 + \frac{0.62 Re_d^{1/2} Pr^{1/3}}{1 + (0.4/Pr)^{2/3})^{1/4}} \cdot (1 + (\frac{Re_d}{282000})^{5/8})^{4/5}$$

\bar{Nu}_d , the Churchill-Berstein average value of the Nusselt number, where Re_d is the Reynolds number and Pr is the Prandtl number. Re_d an dimensionless number depending on the geometry of the object :

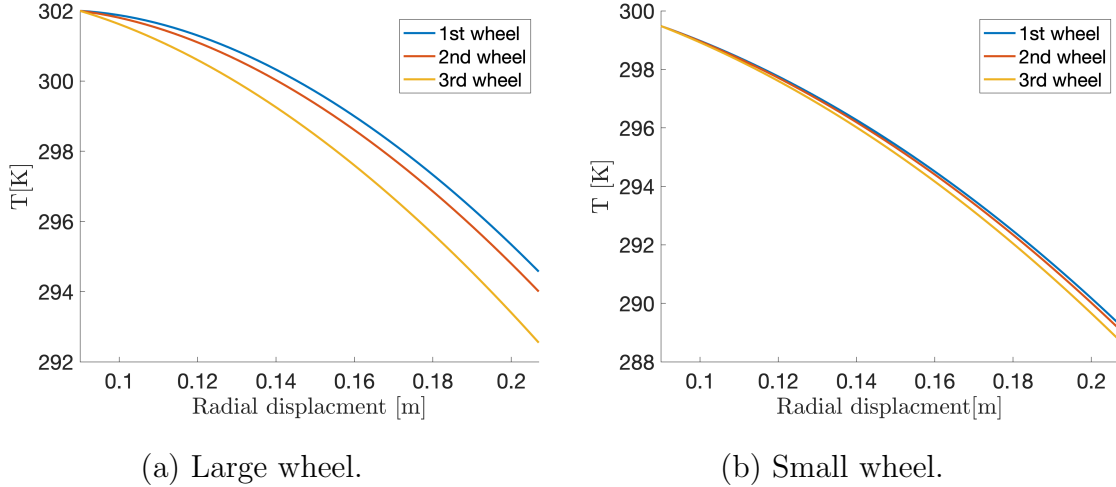
$$Re_d = \frac{\rho \cdot \omega \cdot R_{max} \cdot D}{\mu_{air}} = \frac{\rho \cdot v \cdot D}{\mu_{air}}$$

The Prandtl number, depends only on the thermal properties of the fluid and is constant : $Pr = 0.708$.

After computing the Nusselt number (Nu_d for a cylinder), we can find the convection coefficient depending on the rotational speed. C_1 is resolved. Secondly, by using the boundary condition of Dirichlet (see §8 figure 28), we can compute C_2 :

$$C_2 = T(R_{max}) = T_s$$

Figure 16: Conduction thought the wheels.



Starting from the extreme radius point (0.09 m) and going towards the center of the wheel.

Both graphs start at the extreme radius of both gears. One can see that all the temperatures decrease rapidly, hence the conduction does not have an affect the other side of both gears. Also, the temperature can reach values below the ambient temperature (lower than 295.65 K), which by the thermodynamics law is not possible. In reality, once this temperature is reached by the radial temperature profile, the wheel temperature is constant and equal to the environmental one. To conclude for each gears, the heat flux due to the friction force between the teeth does not accumulate itself. Therefore, the temperature surface at the contact does not change in time. The heat transfer is also the same between every teeth (when velocity increase moment decreases). One can see the same result by the heat camera (see figure 25).

Convection

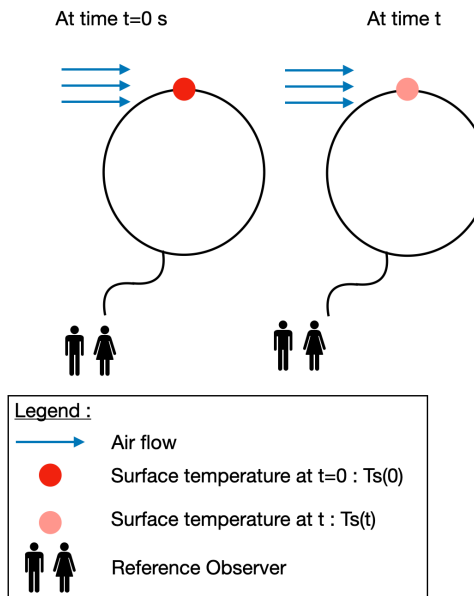
The focus of this section is to determine the temperature profile in a gear wheel due to convection, radial temperature profile of a one-dimension time dependant system.

First, a list of assumption :

- The contact resistance between the teeth are negligible.
- The convection is forced and external.
- The properties of the wood are constant.
- A gear wheel are simplified as cylinder.
- Radiation is neglected (due to the small diffusivity of wood).

- One dimension heat transfer.

Figure 17: Schematic explain the referential change.



For a time depending system the Biot number is required (Bi , a dimensionless number), to determine if this system is a lumped capacitance model ($Bi < 0.1$) or not.

For a cylinder, $Bi = \frac{hR}{k}$ where h is the convection coefficient, (explain and derive in the previous section), R the radius of the cylinder, k the thermal coefficient of the material. For $Bi > 0.1$ the temperature profile is describe by :

$$T(r) = T_a + (T_s - T_a) \cdot A_1 \cdot \exp(-\lambda_1^2 \cdot Fo)$$

With T_a , the environmental temperature, the Fourier's number $Fo = \frac{\alpha \cdot t}{r_0^2}$, λ_1 and A_1 , values interpolated of the figure 29 (§8) that depends on the geometry of the object under convection and the Biot number. For $Bi < 0.1$, the temperature profile is describe by :

$$T(r) = T_a + (T_s - T_a) \cdot \exp(-Bi \cdot Fo)$$

Table 6: Biot number of the largest wheels during the experiments (applied moment $M=5 [N \cdot m^{-1}]$).

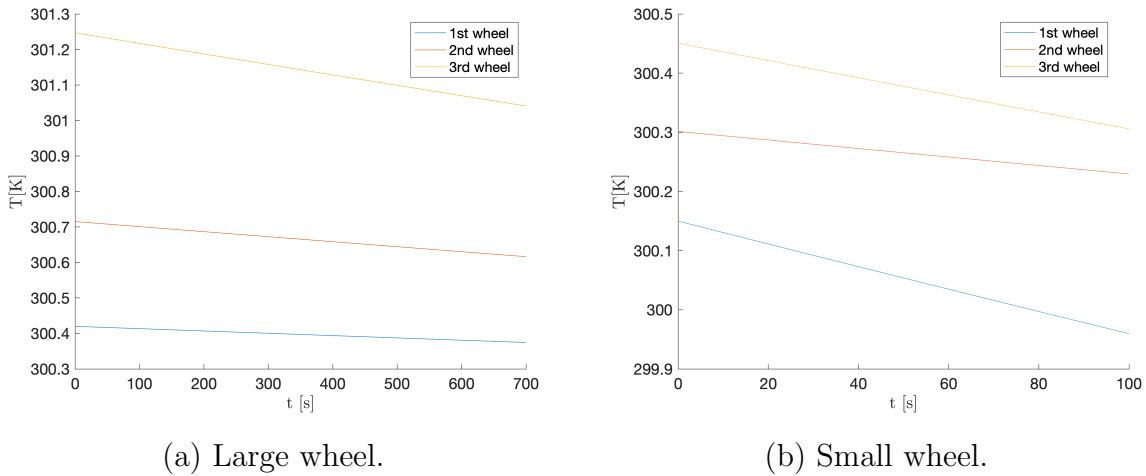
large wheel	1	2	3
rotational speed [$rad \cdot s^{-1}$]	0.8762	4.3812	21.9060
Bi	0.2546	0.5574	1.3349
λ_1	0.6876	0.985	1.3594
A_1	1.06	1.12589	1.24379

Table 7: Biot number of the smallest wheels during the experiments (applied moment $M=5 [N \cdot m^{-1}]$).

small wheel	1	2	3
rotational speed [$rad \cdot s^{-1}$]	0.8762	4.3812	21.9060
Bi	0.0791	0.1456	0.2983
λ_1	-	0.51477	0.72172
A_1	-	1.03366	1.0712

Since $Bi < 0.1$ of the first small wheel, λ_1 and A_1 are not calculated.

Figure 18: Convection through the gears.



In this figure, the temperature profile due to convection decreases in time, but the time range is larger than any time rotation of our wheels. This might be explained because the mathematical method used before requires that Fourier's number Fo , must be greater than 0.2. But, this quantity depends only on time. To conclude this mathematical model is not qualified for our system since we want to analyse the convection effect on small range of time (smaller than one rotation of each wheel).

Heat Generation experiment by contact

The goal of this experiment is to analyze the maximum temperature reached by a maximum friction force of the gear box. The area where the friction force can be maximized is on the last gear, on the furthest point from its center (highest rotational speed reached), by exerting a normal force. We used the data from the experiment to express temperature depending on the rotational speed reached. Then with Matlab, a regression curve was fitted to the data to approximate the required speed for a chosen temperature: $T = f(x) = 0.1757x + 32.8437$.

Figure 19: Generated temperature by contact in respect to angular velocity.

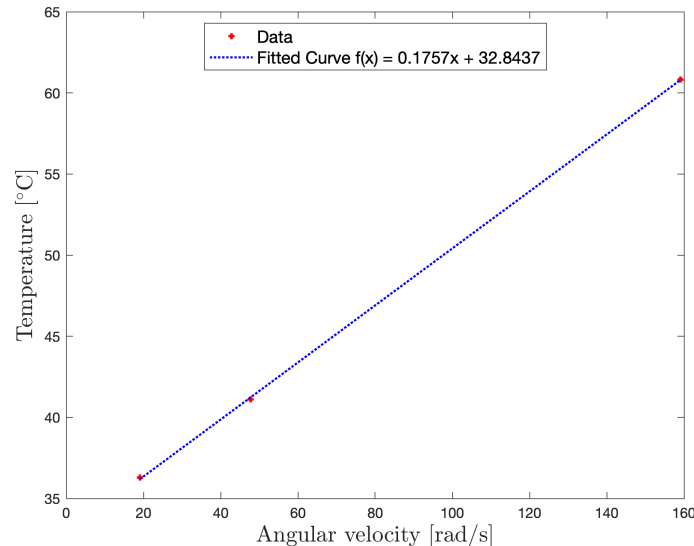
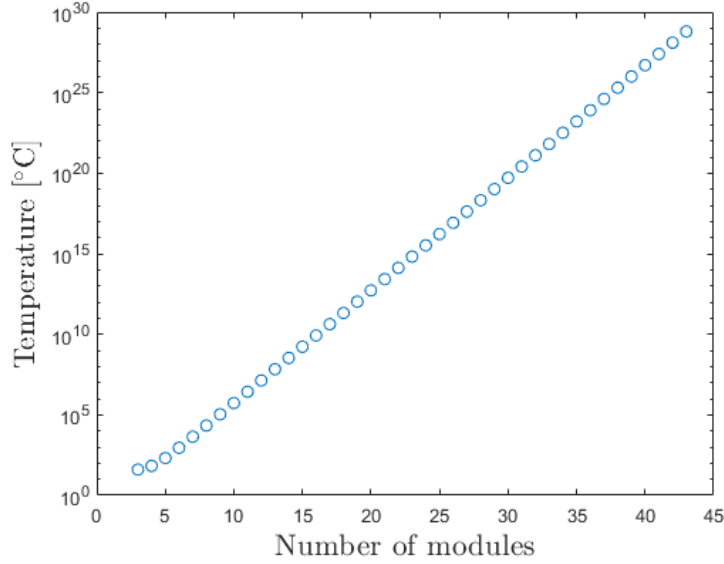


Figure 20: Generated temperature by contact in respect to number of modules for an angular velocity of the first gear of $\frac{\pi}{2} \text{ rad} \cdot \text{s}^{-1}$.



From the expression of the fitted curve, we can for a chosen temperature determine the rotation speed required. For example to reach $T = 150\text{C}^\circ$, the rotation speed must be $\omega = 666.779 \text{ rad} \cdot \text{s}^{-1}$, which occurs with a torque of $185.3N \cdot m^{-1}$, for 4 modules.

To conclude Leonard da Vinci's theory, the temperature of the sun is : $T = 5772K = 5501.85\text{C}^\circ$, the rotation speed must be $\omega = 30'940 \text{ rad} \cdot \text{s}^{-1}$, which implies a torque of $3.99 \cdot 10^5$ for 4 modules. The torque value seems lower than expected. This result may be explained by our small set of data, that is contained in a small range of rotation speed. Since we use MDF, we were limited by the resistance to torsion of this material and could not reach higher rotation velocity. This limitation results in our small set of data.

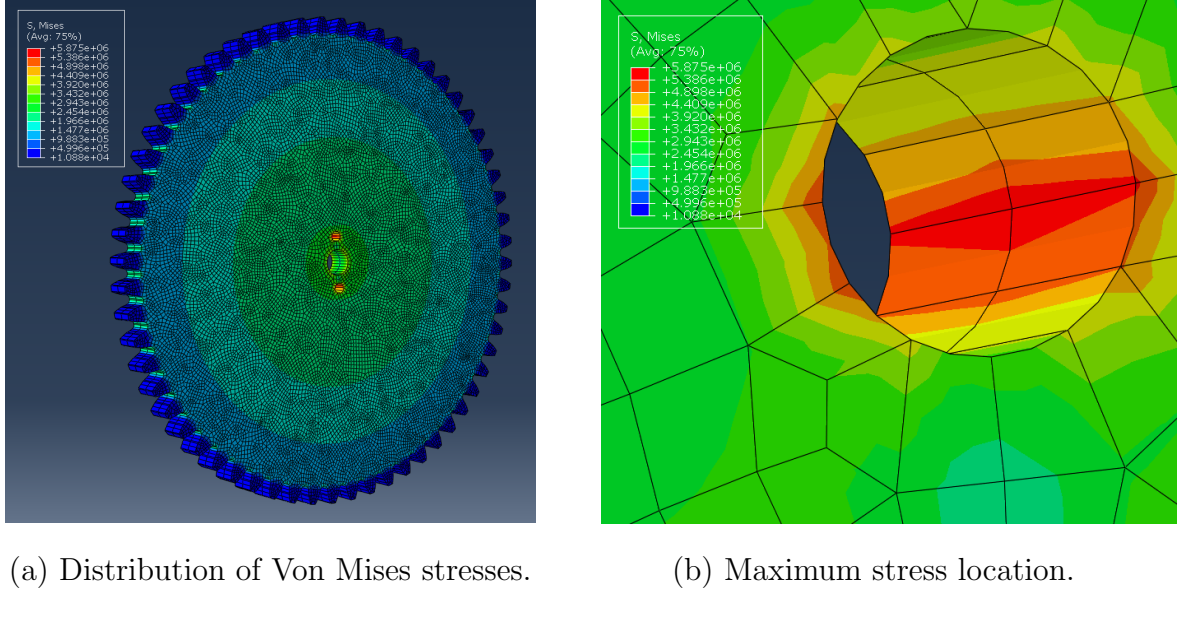
4.1.3 Finite element analysis

In the case of the gearbox, the mechanical parts will limit the maximum rotational speed of the gears. Calculating the point where the gears start breaking under high stresses due to rotation happens to be complex. As shown later on, these speeds range several orders of magnitude above the maximum speed we were able to reach with our setup. This is where FEM enables us to find numerical solutions to find these maximum rotational speeds. The 3D models of the two gears (60-teeth and 12-teeth gears) are imported in the *Abaqus CAE* software and are fitted with the right boundary conditions. The degrees of freedom of the inner hole are blocked and thus each gear is ready for meshing. The material was assumed isotropic which greatly simplifies the analysis despite being a composite material.

In order to prove that the results found are coherent with reality, we show that the values calculated converge with the number of elements (or size of the elements) present in

the mesh. The maximum stress among each gear is used as a test to evaluate the quality of the meshes. These values seem to stabilize beyond approximately 20'000 elements (see figure 17).

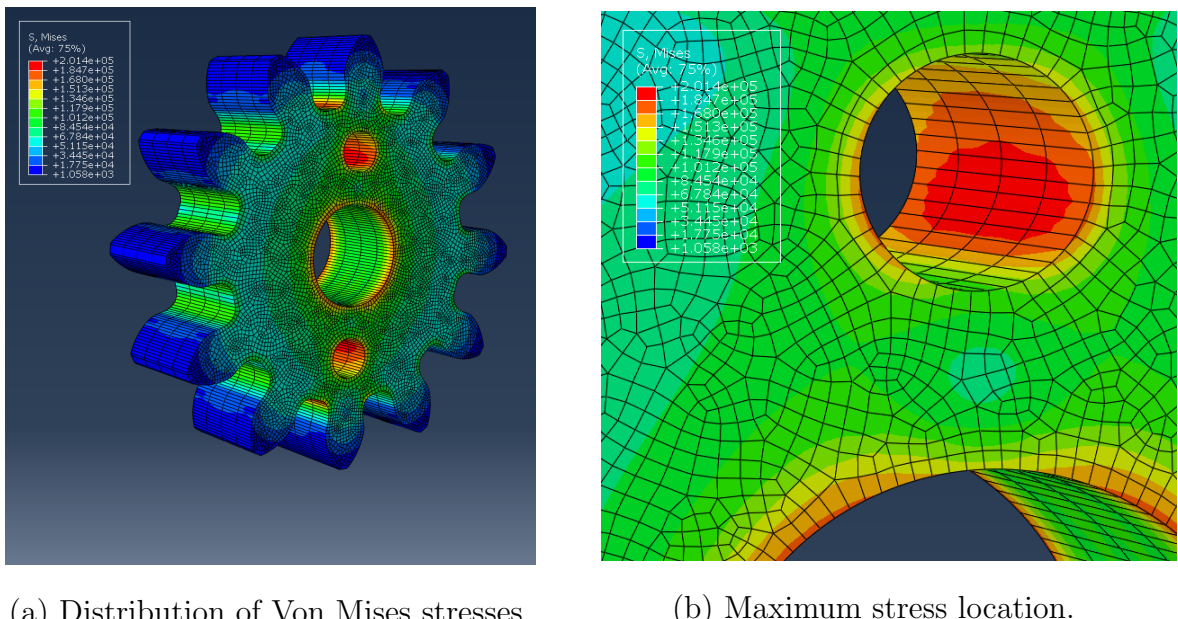
Figure 21: 3D Model of the 60-teeth gear and maximum ($\omega = 1000$ [rad/s]).



(a) Distribution of Von Mises stresses.

(b) Maximum stress location.

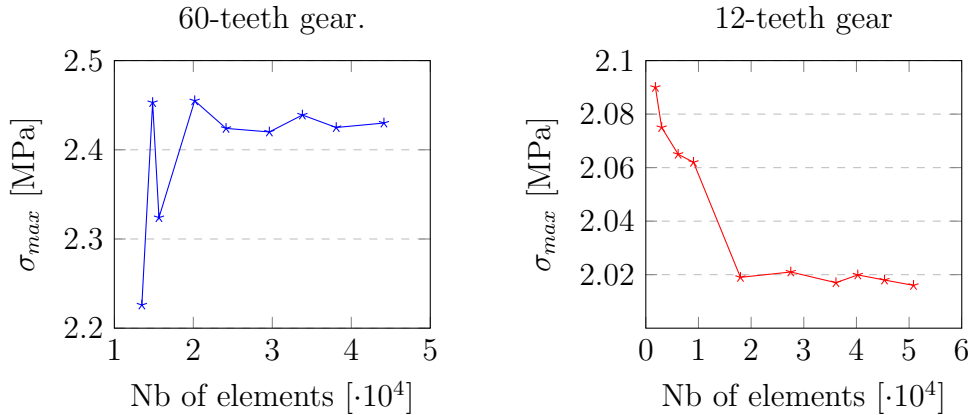
Figure 22: 3D Model of the 12-teeth gear and maximum ($\omega = 1000$ [rad/s]).



(a) Distribution of Von Mises stresses.

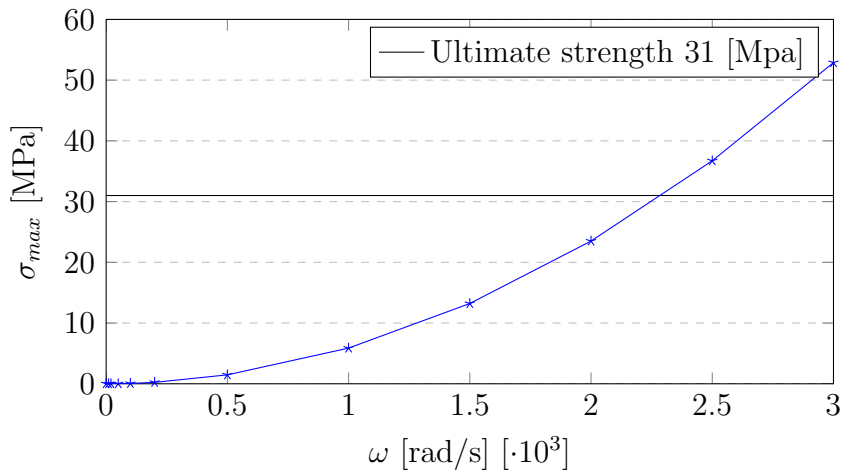
(b) Maximum stress location.

Figure 23: Convergence of the 3D models used.



Using the meshes with the smallest finite elements allowed by *Abaqus CAE* for each gear we can see where the maximum stresses, located on the pin holes where the screws would fit, reach the ultimate strength of MDF thus rupturing the gear.

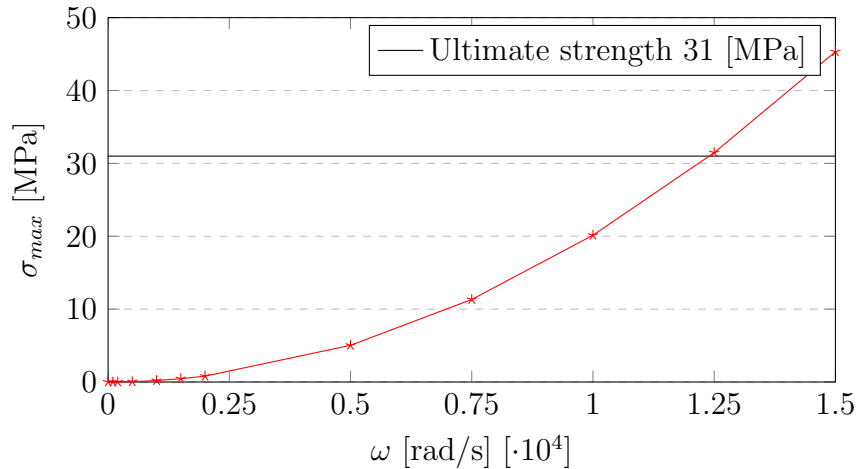
Figure 24: Maximum stress on the 60-teeth gear.



Interestingly, the graph follows approximately the following equation:

$$\sigma_{max} \approx 5.875 \cdot \omega^2$$

Figure 25: Maximum stress on the 12-teeth gear.



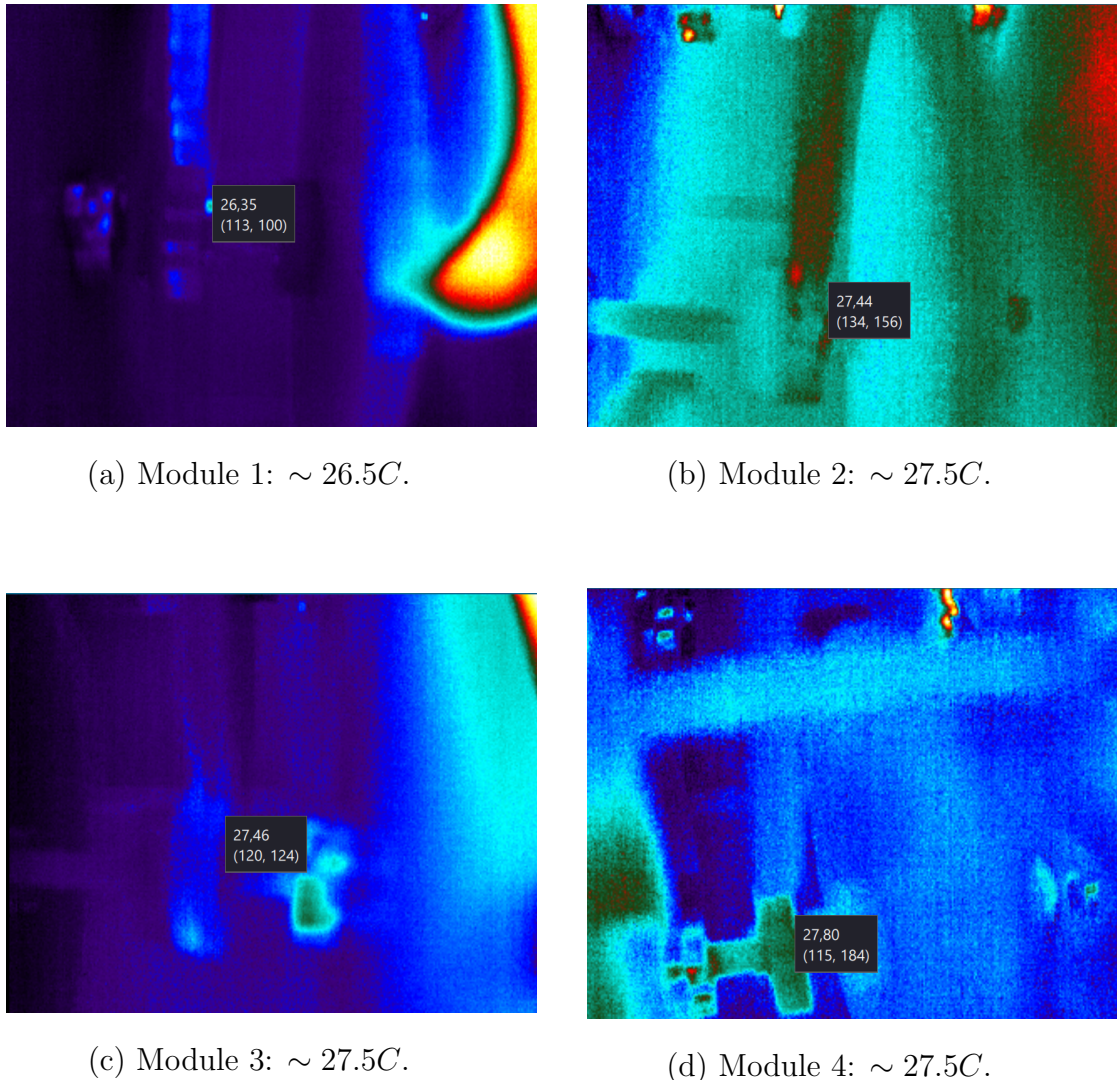
Same case, where the 12-teeth gear follows this following equation:

$$\sigma_{max} \approx 0.2014 \cdot \omega^2$$

The ultimate speed ω_{max} for each gear can be found by inverting the two expressions. We obtain 2'297.08 [rad/s] for the 60-teeth gear and 12'406.55 [rad/s] for the 12-teeth gear. This is perfectly normal as the big gear have more mass and more volume "pulling" on the maximum stress location, lowering considerably the maximum usable speed.

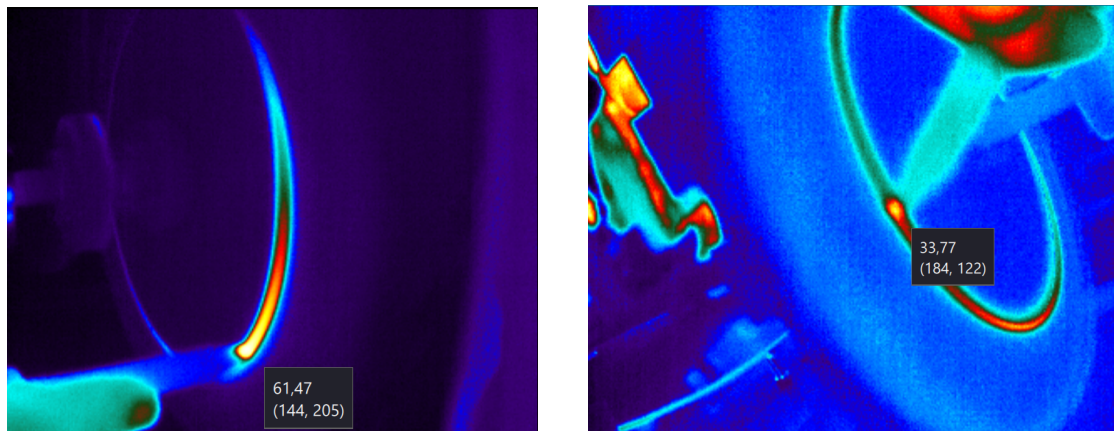
4.2 Results

Figure 26: Images of the temperatures measured on the contact points between the gears.



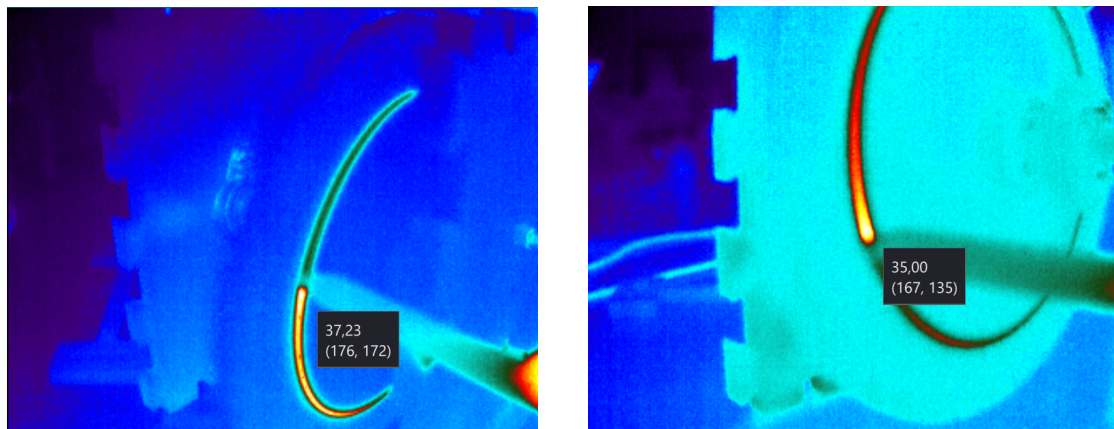
We notice that the temperatures are globally the same independently of the modules. The small angular velocity of the first module might leave more time for the teeth to cool down and thus slightly lowering the surface temperature.

Figure 27: Images of the temperatures measured on their respective modules.



(a) Module 4: rotation speed ≈ 17 [rotation/s].

(b) Module 3: rotation speed ≈ 5 [rotation/s].



(c) Module 2: rotation speed ≈ 5 [rotation/s].

(d) Module 1: rotation speed ≈ 2 [rotation/s].

5 Conclusion

The objective of this study was to investigate the feasibility of Leonardo da Vinci's gear box design. Through our analysis, we discovered that our version of his idea required an amount of power surpassing what may even be physically possible. Consequently, it is evident that da Vinci's thought experiment is impossible to implement due to the prohibitively large power requirements.

It is important to exercise caution when interpreting these results, as numerous assumptions were made to facilitate the analysis. While da Vinci's gear box concept proves unfeasible for practical applications, this study highlights the potential benefits of conducting more precise analysis in the prediction of heat generated by gears in industrial systems. Traditionally, heat generation and friction in this field is determined empirically rather than theoretically. Further research in this area could provide valuable insights into more accurate predictions of heat generation and inform the design of efficient gear systems.

Interestingly, our investigation also revealed that da Vinci's idea was particularly incorrect in terms of gear configuration. It was surprising to find that utilizing a smaller set of gears proved to be more effective in generating higher angular velocity output and therefore temperatures , between a gear and a contacting object, with the same input torque .

In summary, while da Vinci's gear box design is unworkable due to the immense power requirements, this study sheds light on the importance and complexity of precise analysis for predicting heat generation in industrial gear systems. Future research can build upon these findings to enhance the efficiency and performance of gear systems in various applications as well as further improve modeling of friction.

6 Acknowledgement

Special thanks to Professor Pedro M. Reis for the project, our Teaching Assistant Fani Derveni for her precious help, Professor J.F. Molinari for his expertise on friction, Mahendra Patel and the LRESE Lab for the thermal camera and Ivan Tomic as laser cutting chief executor.

7 Bibliography

- Article on friction : Coulomb, Tresca and Coulomb-Tresca friction models used in analytical analysis for rolling process of external spline by Da-Wei Zhang a, Fang-Fang Xu a, Zai-Chi Yu a, Kun-Yin Lu a, Ze-Bang Zheng b, Sheng-Dun Zhao.
- Nasa drag equation.
- Energy output of GRB 130427A.
- Measurement of Gear Tooth Dynamic Friction.
- Analyse des pertes de puissance dans les transmissions par engrenages à grande vitesse. Applications aux réducteurs industriels et aux machines textiles .
- Analytical and experimental investigation of rake contact and friction behavior in metal cutting by Emre Ozlu , Erhan Budak , A. Molinari.
- Books from the Rolex Learning Center : (texts, drawings of Leonardo da Vinci).
- Le fantastiche macchine di Leonardo da Vinci : come costruirle, come farle funzionare Milano : Skira ; Museo nazionale della scienza e della tecnica Leonardo da Vinci 1999.
- Léonard de Vinci la nature et l'invention sous la dir. de Patrick Boucheron et Claudio Giorgione Boucheron, Patrick.
- Léonard de Vinci ingénieur et architecte ; [sous la dir. de Paolo Galluzzi] Galluzzi, Paolo.
- Courses from EPFL
 - Heat and Mass transfer, Pr.G.Tagliabue.
 - Système Méchanique, Pr.S.Soubielle.

8 Appendix

Figure 28: Boundary Conditions

Boundary Conditions (BCs)	1 st Kind (Dirichlet)	2 nd kind (Neumann)	3 rd kind (Robin)
	$T(x_i, y_i, z_i) = T_s$	$-k \left(\frac{\partial T}{\partial x} \right)_{x=x_i} = q_s''$	$-k \left(\frac{\partial T}{\partial x} \right)_{x=x_i} = h(T(x_i, t) - T_\infty)$

Table from Heat and mass transfer, Pr G. Tagliabue

Figure 29: Physical properties A_1 and λ_1 depending on the Biot number

Bi	Plate			Cylinder			Sphere		
	$\hat{\lambda}_1$	A_1	D_1	$\hat{\lambda}_1$	A_1	D_1	$\hat{\lambda}_1$	A_1	D_1
0.01	0.09983	1.0017	1.0000	0.14124	1.0025	1.0000	0.17303	1.0030	1.0000
0.02	0.14095	1.0033	1.0000	0.19950	1.0050	1.0000	0.24446	1.0060	1.0000
0.05	0.22176	1.0082	0.9999	0.31426	1.0124	0.9999	0.38537	1.0150	1.0000
0.10	0.31105	1.0161	0.9998	0.44168	1.0246	0.9998	0.54228	1.0298	0.9998
0.15	0.37788	1.0237	0.9995	0.53761	1.0365	0.9995	0.66086	1.0445	0.9996
0.20	0.43284	1.0311	0.9992	0.61697	1.0483	0.9992	0.75931	1.0592	0.9993
0.30	0.52179	1.0450	0.9983	0.74646	1.0712	0.9983	0.92079	1.0880	0.9985
0.40	0.59324	1.0580	0.9971	0.85158	1.0931	0.9970	1.05279	1.1164	0.9974
0.50	0.65327	1.0701	0.9956	0.94077	1.1143	0.9954	1.16556	1.1441	0.9960
0.60	0.70507	1.0814	0.9940	1.01844	1.1345	0.9936	1.26440	1.1713	0.9944
0.70	0.75056	1.0918	0.9922	1.08725	1.1539	0.9916	1.35252	1.1978	0.9925
0.80	0.79103	1.1016	0.9903	1.14897	1.1724	0.9893	1.43203	1.2236	0.9904
0.90	0.82740	1.1107	0.9882	1.20484	1.1902	0.9869	1.50442	1.2488	0.9880
1.00	0.86033	1.1191	0.9861	1.25578	1.2071	0.9843	1.57080	1.2732	0.9855
1.10	0.89035	1.1270	0.9839	1.30251	1.2232	0.9815	1.63199	1.2970	0.9828
1.20	0.91785	1.1344	0.9817	1.34558	1.2387	0.9787	1.68868	1.3201	0.9800
1.30	0.94316	1.1412	0.9794	1.38543	1.2533	0.9757	1.74140	1.3424	0.9770
1.40	0.96655	1.1477	0.9771	1.42246	1.2673	0.9727	1.79058	1.3640	0.9739
1.50	0.98824	1.1537	0.9748	1.45695	1.2807	0.9696	1.83660	1.3850	0.9707

Table from Heat and mass transfer, Pr G. Tagliabue

Figure 30: Thermophysical Properties of Air at atmospheric pressure

TABLE A.4 Thermophysical Properties of Gases at Atmospheric Pressure^a

T (K)	ρ (kg/m ³)	c_p (kJ/kg · K)	$\mu \cdot 10^7$ (N · s/m ²)	$\nu \cdot 10^6$ (m ² /s)	$k \cdot 10^3$ (W/m · K)	$\alpha \cdot 10^6$ (m ² /s)	Pr
Air							
100	3.5562	1.032	71.1	2.00	9.34	2.54	0.786
150	2.3364	1.012	103.4	4.426	13.8	5.84	0.758
200	1.7458	1.007	132.5	7.590	18.1	10.3	0.737
250	1.3947	1.006	159.6	11.44	22.3	15.9	0.720
300	1.1614	1.007	184.6	15.89	26.3	22.5	0.707

Table from Heat and mass transfer, Pr G. Tagliabue

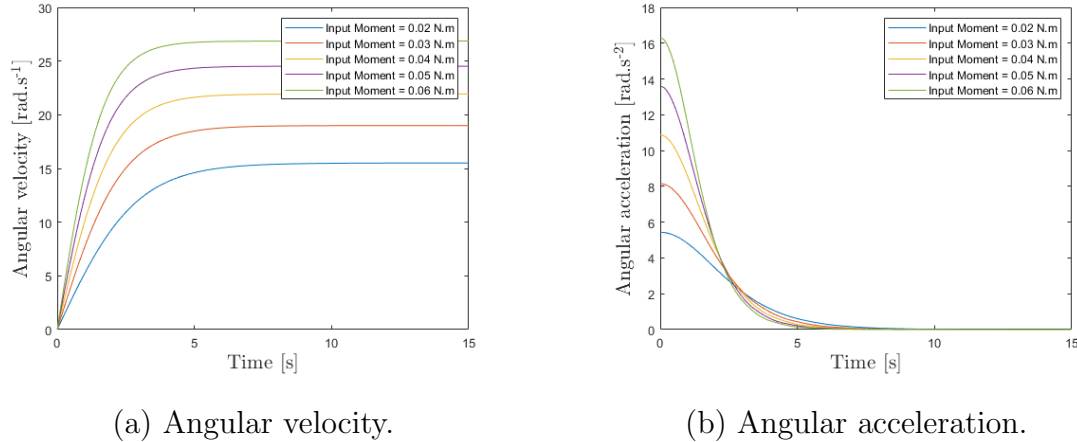
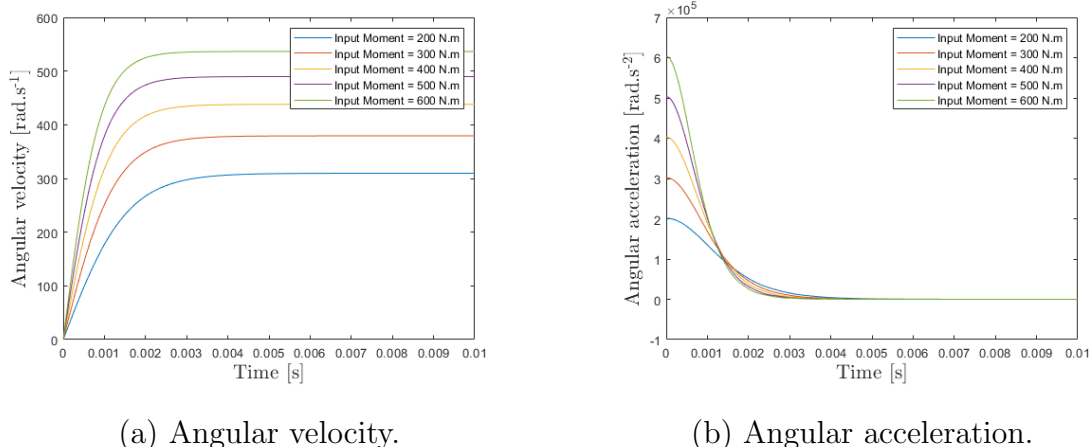
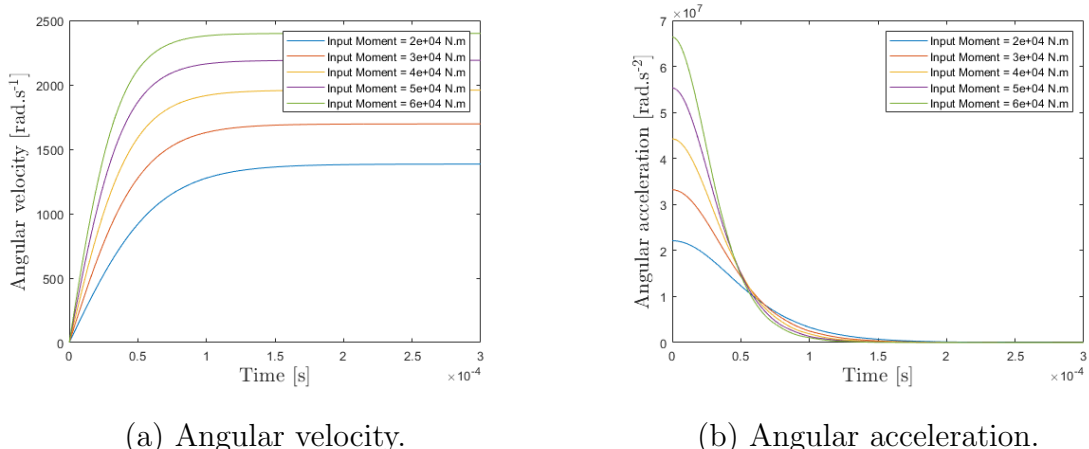
Figure 31: Angular velocity and acceleration for $n = 3$ modules.Figure 32: Angular velocity and acceleration for $n = 5$ modules.Figure 33: Angular velocity and acceleration for $n = 6$ modules.

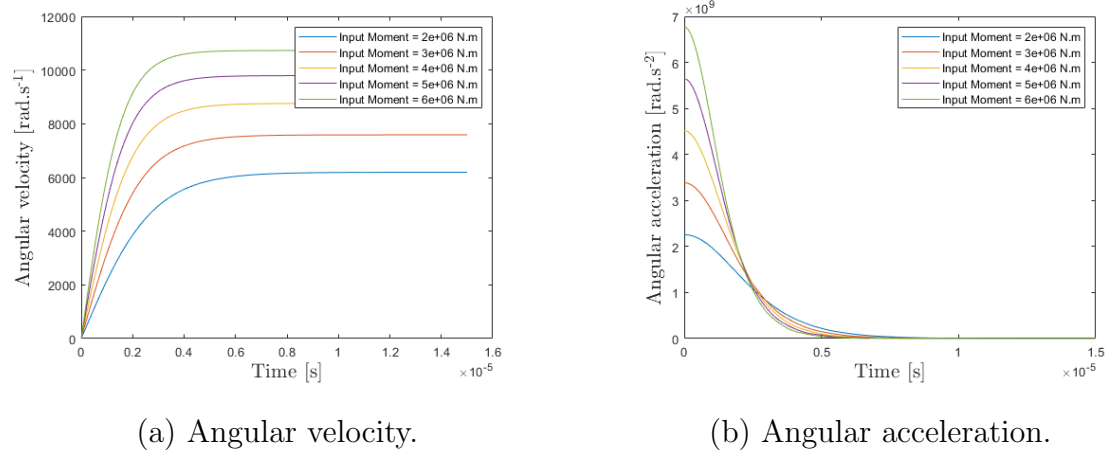
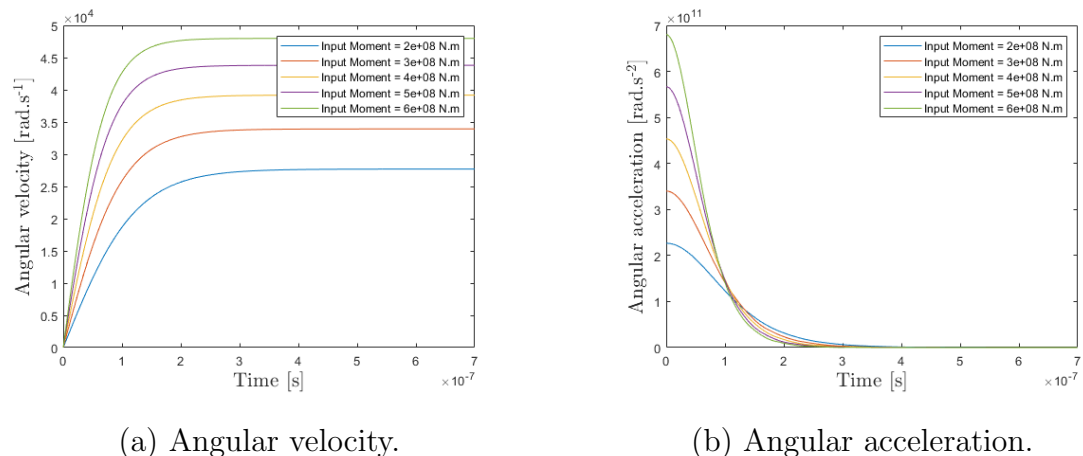
Figure 34: Angular velocity and acceleration for $n = 7$ modules.Figure 35: Angular velocity and acceleration for $n = 8$ modules.

Figure 36: Original page from the Codex Atlanticus

